Electronic Supplementary Material (ESI) for Materials Chemistry Frontiers.


Supporting Materials for

# Interface-Engineered Charge Separation at Selective Electron Tunneling Heterointerfaces

Chunhui Gu,‡[a] Chuancheng Jia‡[a] and Xuefeng Guo*[ab]

[a.] Beijing National Laboratory for Molecular Sciences, State Key Laboratory for Structural Chemistry of Unstable and Stable Species, College of Chemistry and Molecular Engineering, Peking University, Beijing 100871, P. R. China.
E-mail: guoxf@pku.edu.cn

[b.] Department of Materials Science and Engineering, College of Engineering, Peking University, Beijing 100871, P. R. China.

‡ These authors contributed equally to this work.

## Table of Contents

# I. Morphology & optics characterization

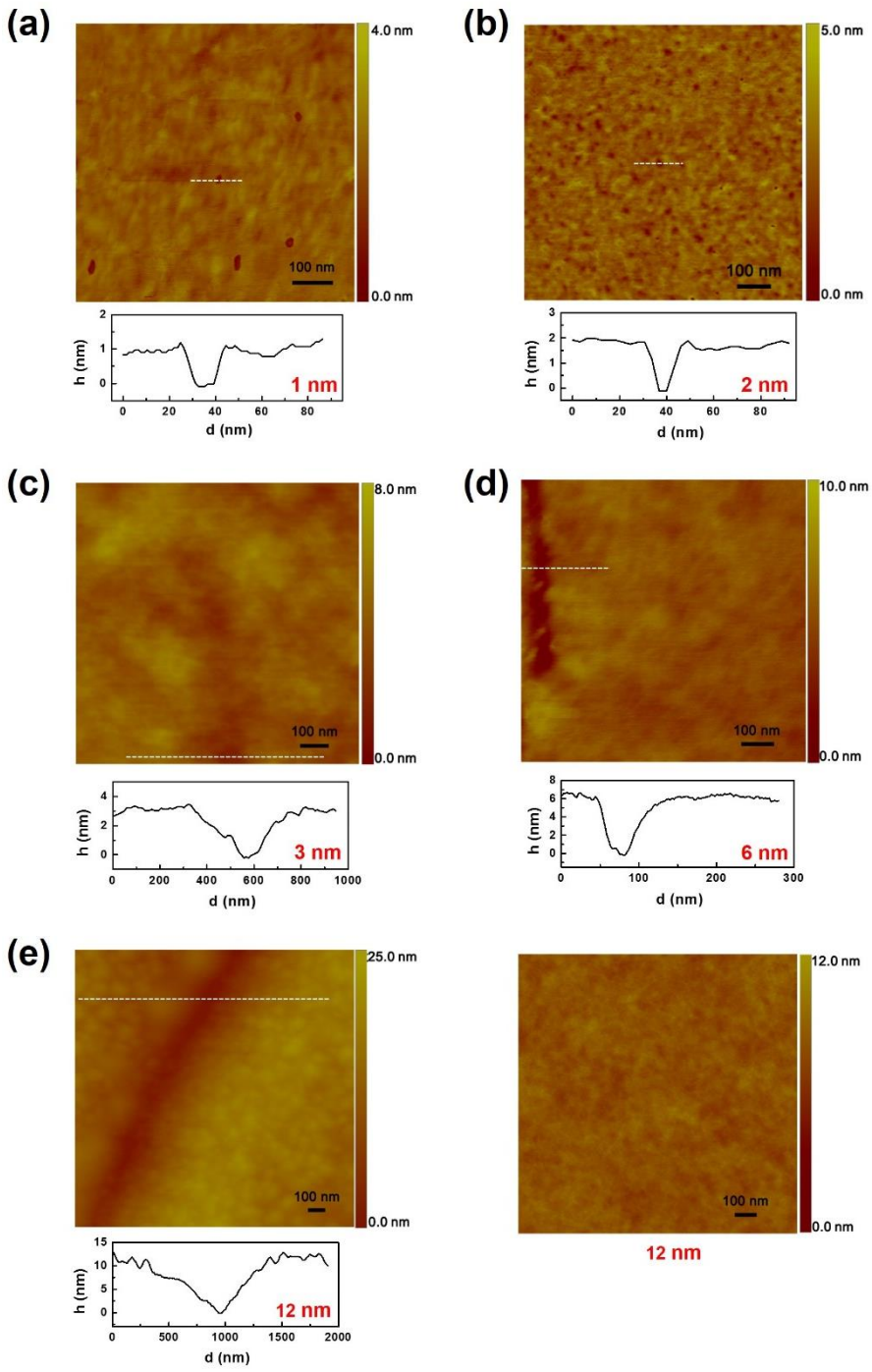


**Fig. S1** Surface morphologies of the $TiO_2$/Gr/Ado ternary interfaces of five samples with different Ado thicknesses. For each sample, the thickness of uniform high-coverage Ado monolayers is obtained from a selected defect. (a-e) shows that the thicknesses of the Ado layer are ~1 nm, ~2 nm, ~3 nm, ~6 nm and ~12 nm, respectively. For ~12 nm Ado, an artifact place (left side of Fig. S1e) is selected for measuring the thickness of the film; and the routine surface of ~12 nm Ado is shown in the right side of Fig. S1e.

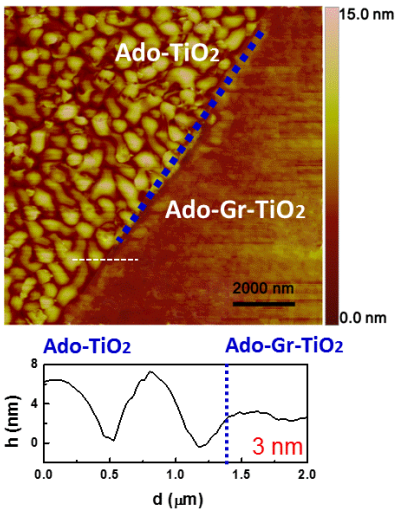


**Fig. S2** Surface morphology of the $TiO_2$/Gr/Ado ternary interface and the $TiO_2$/Ado interface. In comparison with $TiO_2$, Ado is more flatly arranged on the surface of graphene

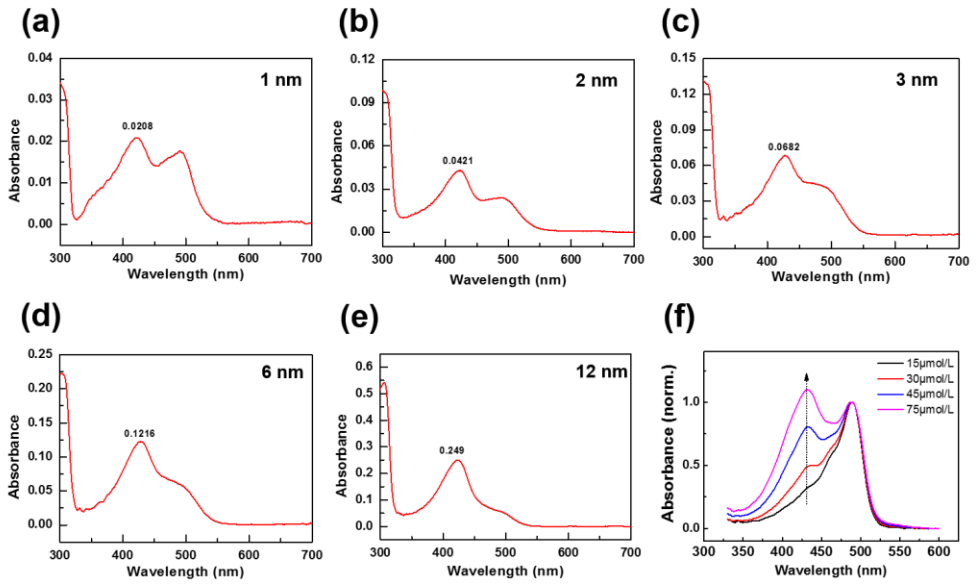


**Fig. S3** (a-e) Absorption spectra of the Ado layers on graphene, in which Ado thicknesses is ~1 nm, ~2 nm, ~3 nm, ~6 nm and ~12 nm. (f) Absorption spectra of Ado in an ethanol solution normalized by the absorption at 489 nm. The absorption peak at 430 nm increases along with the concentration of Ado, which indicates that the absorption is aggregation-induced.

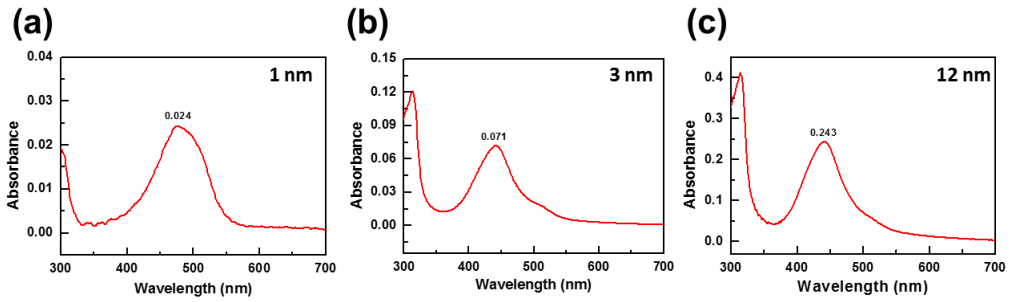


**Fig. S4** Absorption of the Ado/quartz layers with Ado thicknesses of ~1 nm (a), ~3 nm (b), and 12 nm (c).

## II. Optoelectronic characterization

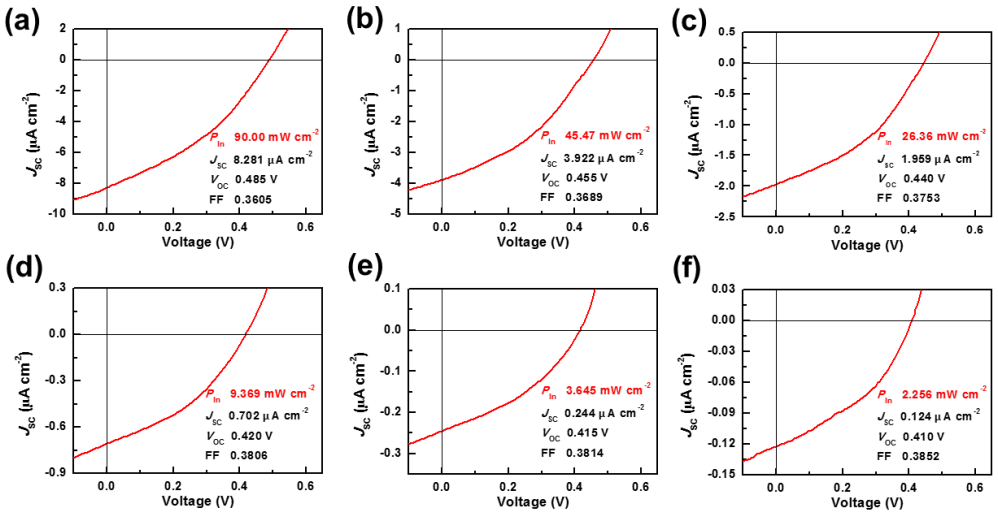


**Fig. S5** Current-voltage characteristics of a $TiO_2$/Gr/Ado (~1 nm) device under different visible light illumination. (a) At the light intensity of 90.00 mW·cm$^{-2}$. (b) At the light intensity of 45.47 mW·cm$^{-2}$. (c) At the light intensity of 26.36 mW·cm$^{-2}$. (d) At the light intensity of 9.369 mW·cm$^{-2}$. (e) At the light intensity of 3.645 mW·cm$^{-2}$. (f) At the light intensity of 2.256 mW·cm$^{-2}$.

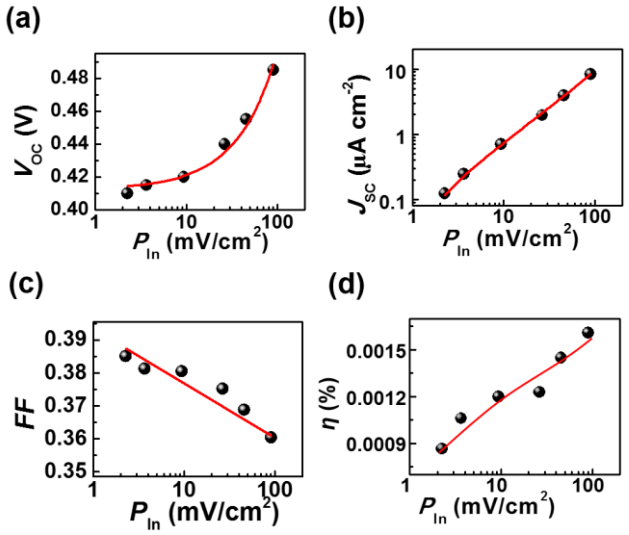


**Fig. S6** Illumination intensity dependence of the device in Fig. S5 measured under visible light illumination. (a) Open circuit voltage ($V_{oc}$) -light intensity dependence. (b) Short current ($J_{sc}$) - light intensity dependence. (c) Fill factor ($FF$) - light intensity dependence. (d) Efficiency ($\eta$) - light intensity dependence.

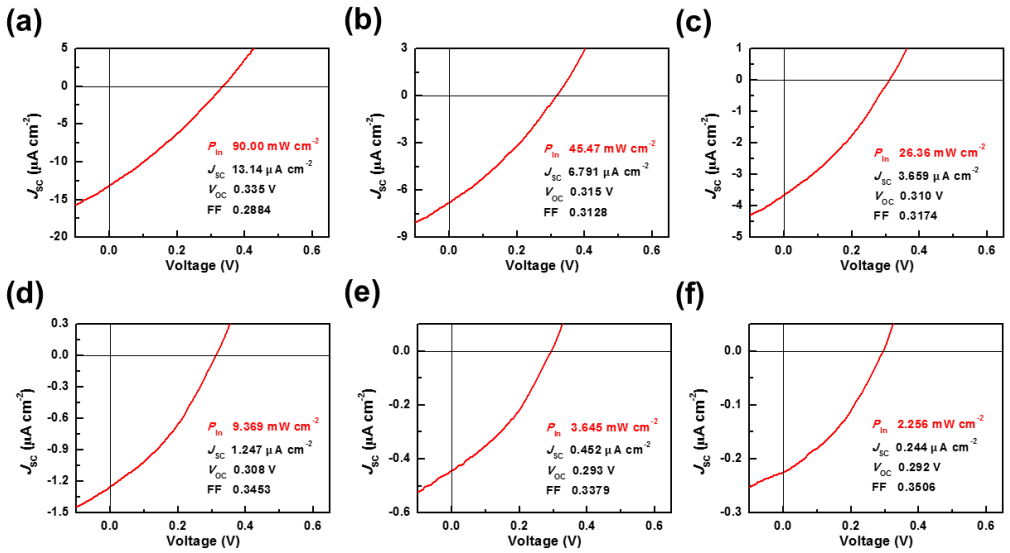


**Fig. S7** Current-voltage characteristics of a $TiO_2$/Gr/Ado (~3 nm) device under different visible light illumination. (a) At the light intensity of 90.00 mW·cm$^{-2}$. (b) At the light intensity of 45.47 mW·cm$^{-2}$. (c) At the light intensity of 26.36 mW·cm$^{-2}$. (d) At the light intensity of 9.369 mW·cm$^{-2}$. (e) At the light intensity of 3.645 mW·cm$^{-2}$. (f) At the light intensity of 2.256 mW·cm$^{-2}$.

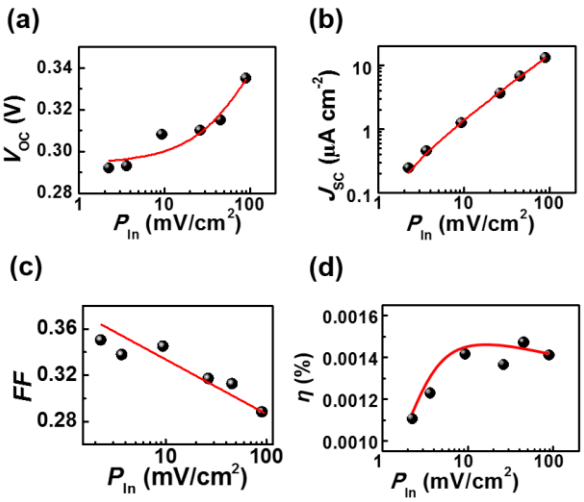


**Fig. S8** Illumination intensity dependence of the device in Fig. S7 measured under visible light illumination. (a) Open circuit voltage ($V_{oc}$) -light intensity dependence. (b) Short current ($J_{sc}$) - light intensity dependence. (c) Fill factor ($FF$) - light intensity dependence. (d) Efficiency ($\eta$) - light intensity dependence.

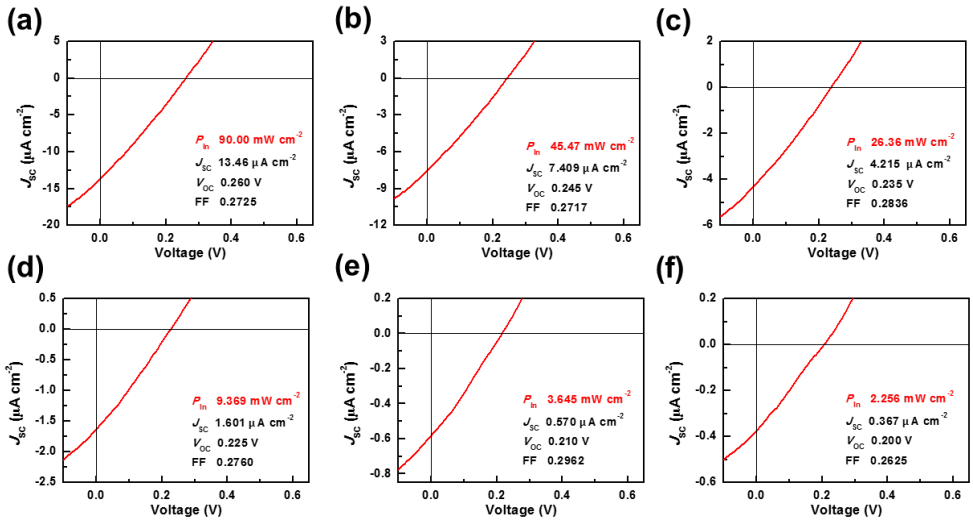


**Fig. S9** Current-voltage characteristics of a $TiO_2$/Gr/Ado (~6 nm) device under different visible light illumination. (a) At the light intensity of 90.00 mW·cm$^{-2}$. (b) At the light intensity of 45.47 mW·cm$^{-2}$. (c) At the light intensity of 26.36 mW·cm$^{-2}$. (d) At the light intensity of 9.369 mW·cm$^{-2}$. (e) At the light intensity of 3.645 mW·cm$^{-2}$. (f) At the light intensity of 2.256 mW·cm$^{-2}$.

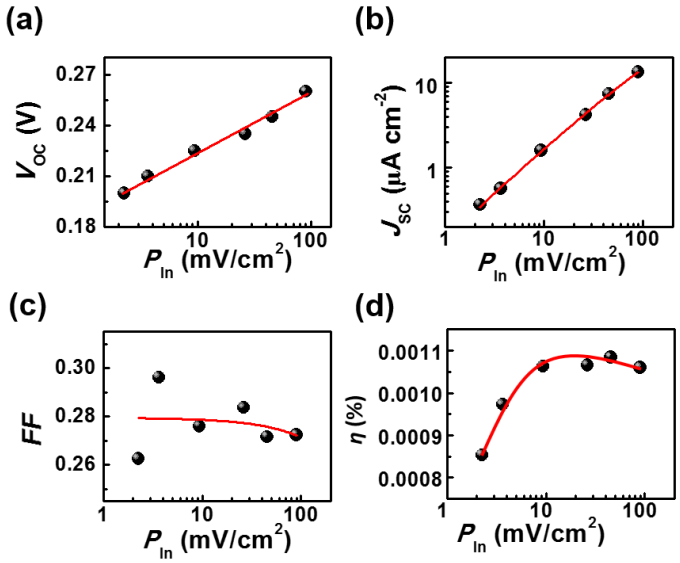


**Fig. S10** Illumination intensity dependence of the device in Fig. S9 measured under visible light illumination. (a) Open circuit voltage ($V_{oc}$) -light intensity dependence. (b) Short current ($J_{sc}$) - light intensity dependence. (c) Fill factor ($FF$) - light intensity dependence. (d) Efficiency ($\eta$) - light intensity dependence.

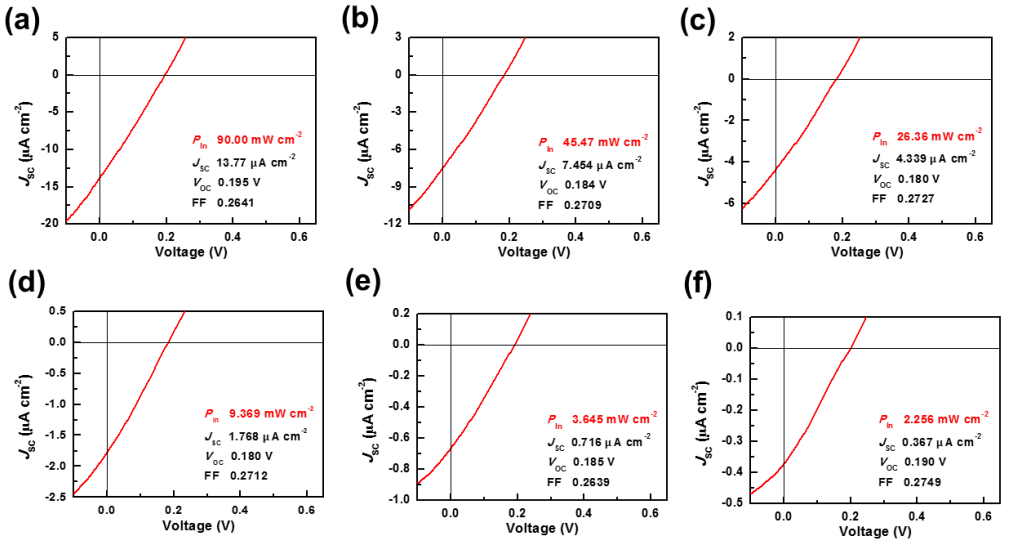


**Fig. S11** Current-voltage characteristics of a $TiO_2$/Gr/Ado (~12 nm) device under different visible light illumination. (a) At the light intensity of 90.00 mW·cm$^{-2}$. (b) At the light intensity of 45.47 mW·cm$^{-2}$. (c) At the light intensity of 26.36 mW·cm$^{-2}$. (d) At the light intensity of 9.369 mW·cm$^{-2}$. (e) At the light intensity of 3.645 mW·cm$^{-2}$. (f) At the light intensity of 2.256 mW·cm$^{-2}$.

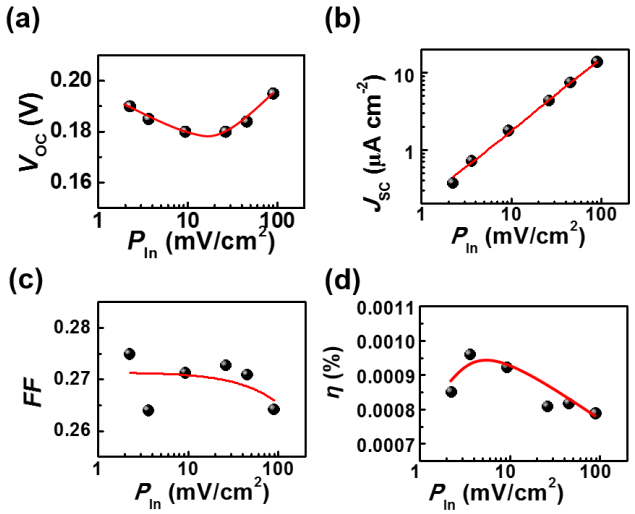


**Fig. S12** Illumination intensity dependence of the device in Fig. S11 measured under visible light illumination. (a) Open circuit voltage ($V_{OC}$) -light intensity dependence. (b) Short current ($J_{SC}$) - light intensity dependence. (c) Fill factor ($FF$) - light intensity dependence. (d) Efficiency ($\eta$) - light intensity dependence.

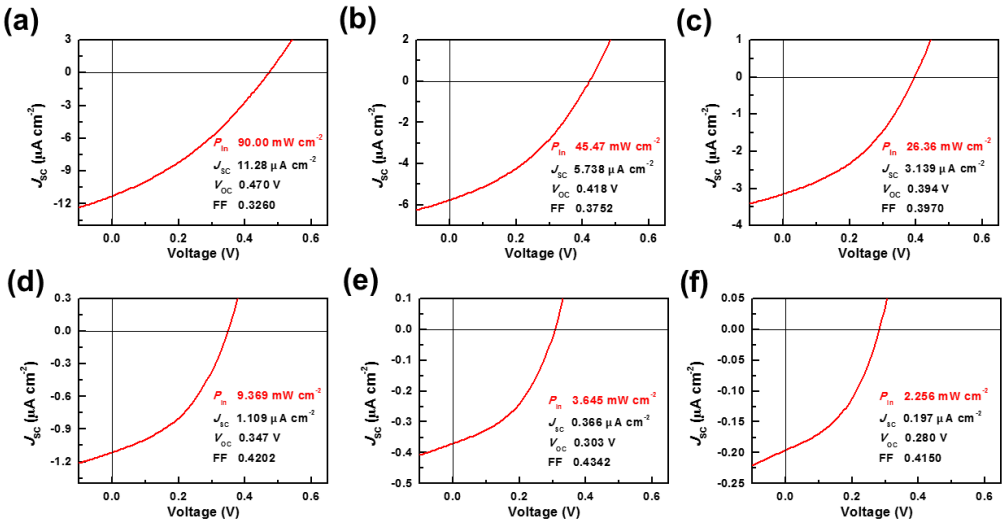


**Fig. S13** Current-voltage characteristics of $TiO_2$/Ado (~1 nm)/Gr Device under different visible light illumination. (a) At the light intensity of 90.00 mW·cm$^{-2}$. (b) At the light intensity of 45.47 mW·cm$^{-2}$. (c) At the light intensity of 26.36 mW·cm$^{-2}$. (d) At the light intensity of 9.369 mW·cm$^{-2}$. (e) At the light intensity of 3.645 mW·cm$^{-2}$. (f) At the light intensity of 2.256 mW·cm$^{-2}$.

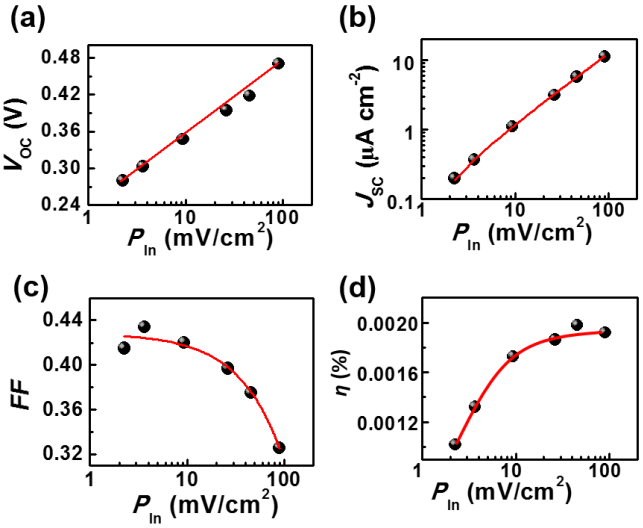


**Fig. S14** Illumination intensity dependence of the device in Fig. S13 measured under visible light illumination. (a) Open circuit voltage ($V_{oc}$) -light intensity dependence. (b) Short current ($J_{sc}$) - light intensity dependence. (c) Fill factor ($FF$) - light intensity dependence. (d) Efficiency ($\eta$) - light intensity dependence.

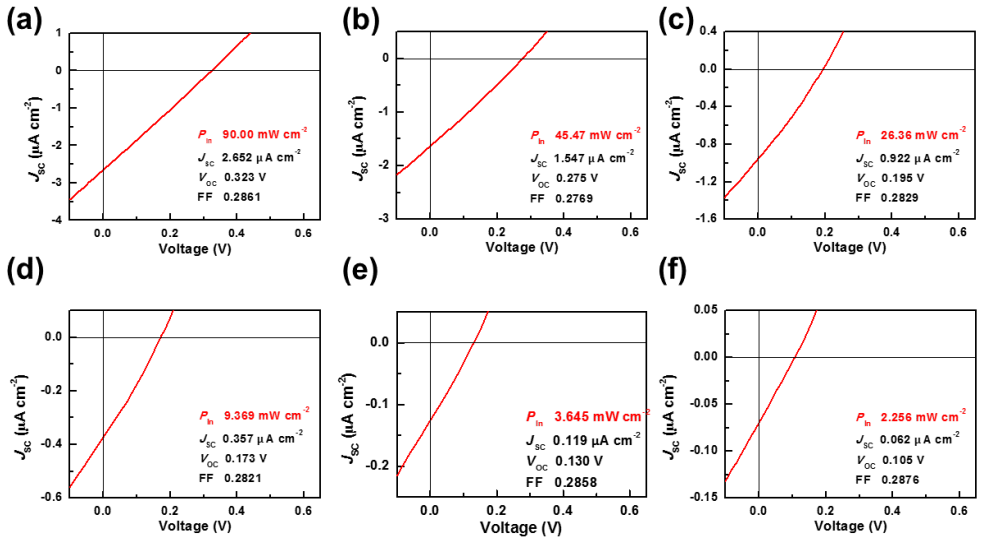


**Fig. S15** Current-voltage characteristics of a $TiO_2$/Ado (~3 nm)/Gr Device under different visible light illumination. (a) At the light intensity of 90.00 mW·cm$^{-2}$. (b) At the light intensity of 45.47 mW·cm$^{-2}$. (c) At the light intensity of 26.36 mW·cm$^{-2}$. (d) At the light intensity of 9.369 mW·cm$^{-2}$. (e) At the light intensity of 3.645 mW·cm$^{-2}$. (f) At the light intensity of 2.256 mW·cm$^{-2}$.

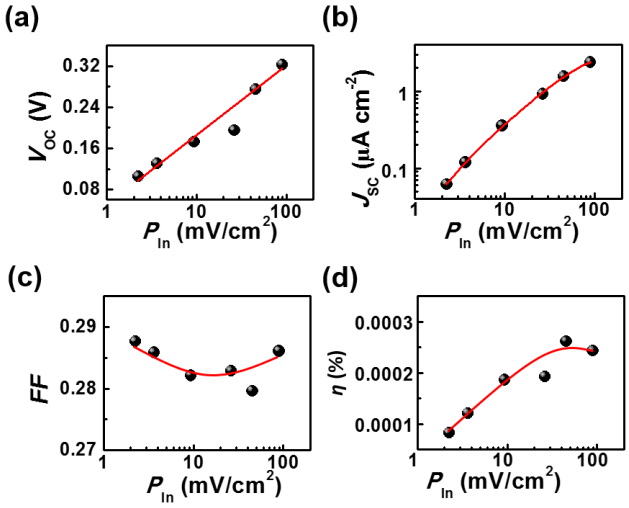


**Fig. S16** Illumination intensity dependence of the device in Fig. S15 measured under visible light illumination. (a) Open circuit voltage ($V_{OC}$) -light intensity dependence. (b) Short current ($J_{SC}$) - light intensity dependence. (c) Fill factor (*FF*) - light intensity dependence. (d) Efficiency ($\eta$) - light intensity dependence.

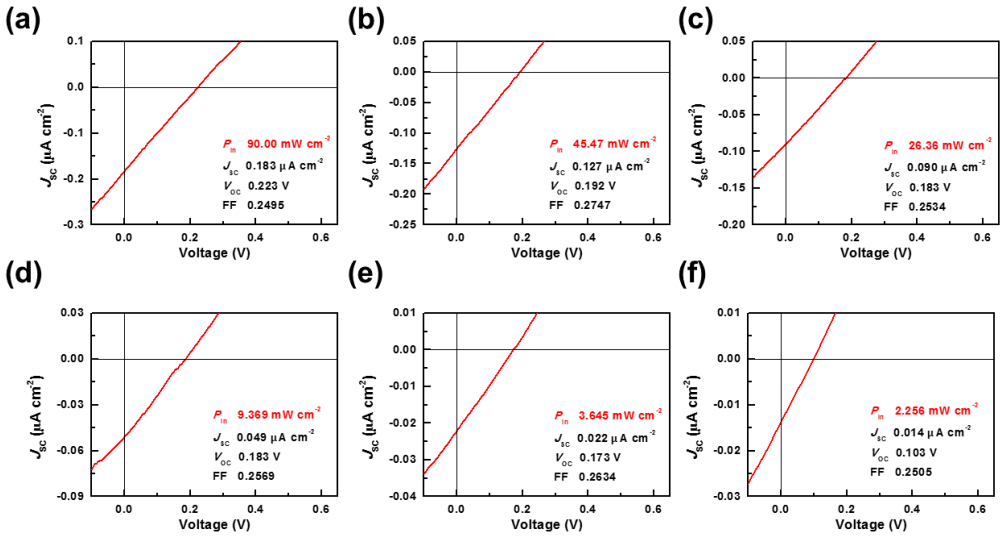


**Fig. S17** Current-voltage characteristics of a $TiO_2$/Ado (~12 nm)/Gr Device under different visible light illumination. (a) At the light intensity of 90.00 mW·cm$^{-2}$. (b) At the light intensity of 45.47 mW·cm$^{-2}$. (c) At the light intensity of 26.36 mW·cm$^{-2}$. (d) At the light intensity of 9.369 mW·cm$^{-2}$. (e) At the light intensity of 3.645 mW·cm$^{-2}$. (f) At the light intensity of 2.256 mW·cm$^{-2}$.

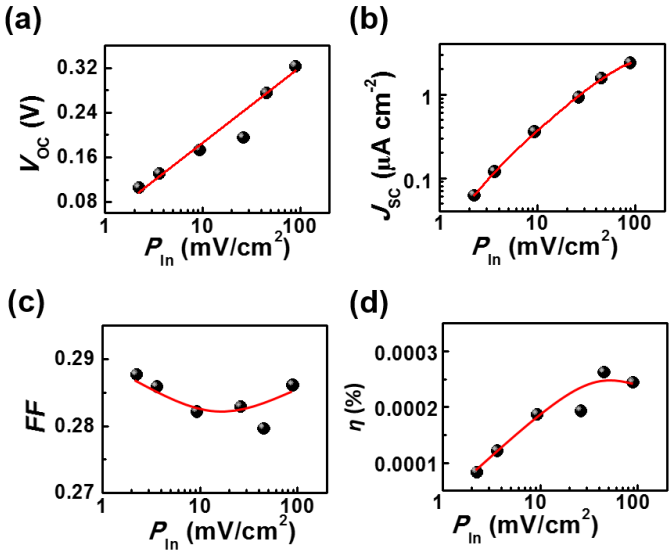


**Fig. S18** Illumination intensity dependence of the device in Fig. S17 measured under visible light illumination. (a) Open circuit voltage ($V_{OC}$) -light intensity dependence. (b) Short current ($J_{SC}$) - light intensity dependence. (c) Fill factor ($FF$) - light intensity dependence. (d) Efficiency ($\eta$) - light intensity dependence.

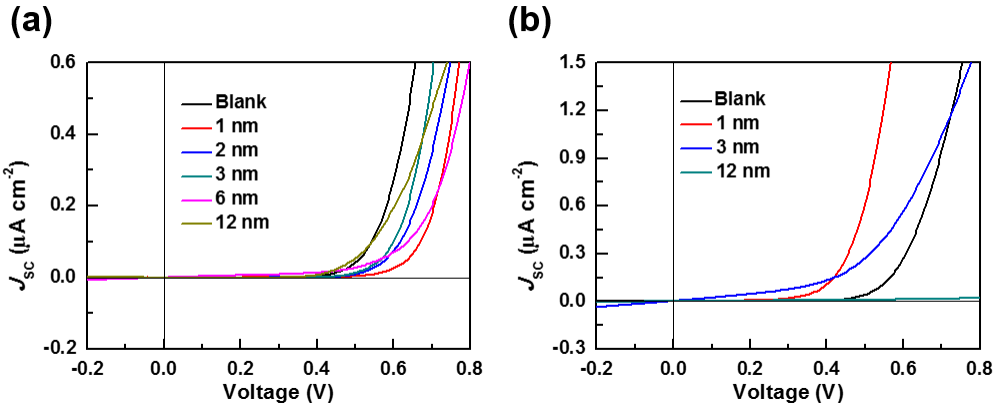


**Fig. S19** Current-voltage characteristics of a $TiO_2$/Gr/Ado structure (a) and a $TiO_2$/Ado/Gr structure (b) with different Ado thicknesses in the dark.

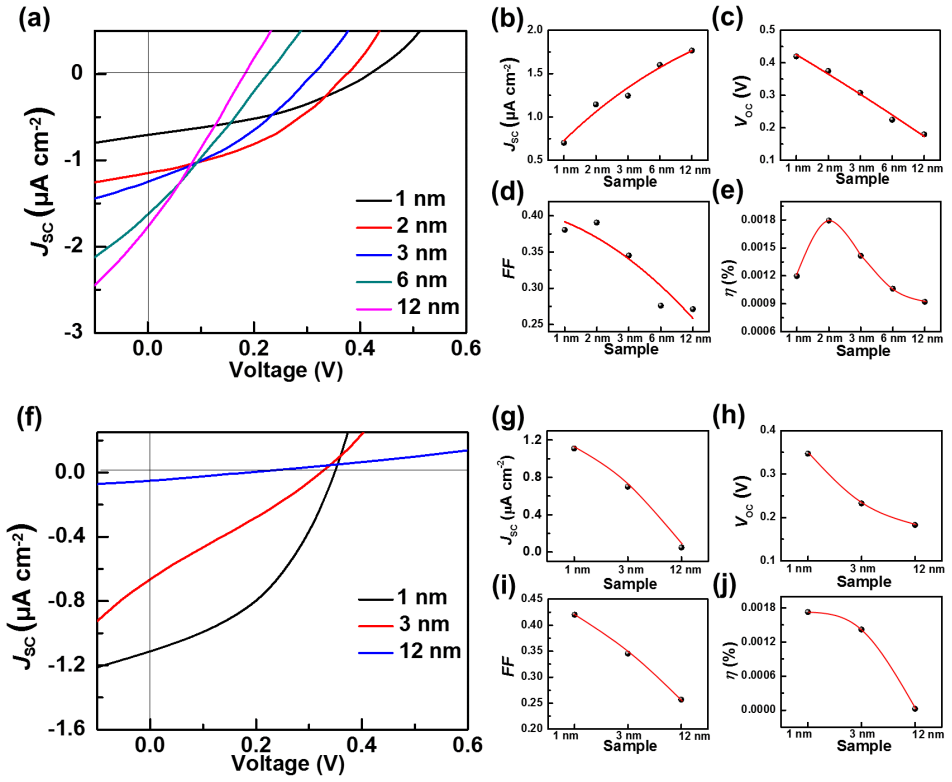


**Fig. S20** Ado thickness-dependent charge separation behaviors under the visible light illumination of 9.369 mW·cm$^{-2}$. (a-e) Current−voltage characteristics (a), open circuit voltage (b), short circuit current (c), fill factor (d) and efficiency (e) of the $TiO_2$/Gr/Ado ternary interface, respectively. (f-j) Current−voltage characteristics (f), open circuit voltage (g), short circuit current (h), fill factor (i) and efficiency (j) of the $TiO_2$/Ado/Gr ternary interface, respectively.

## III. Charge-transfer dynamics characterization

The devices containing the interfaces with the $TiO_2$/Gr/Ado (~1 nm) or $TiO_2$/Gr/Ado (~12 nm) structures were fabricated according to the methods in the Supporting Information above. Time-resolved photoluminescence plots are shown in Fig. S21. The excitation wavelength was set at 473 nm and the PL was measured at 535 nm. The decays of the PL were fitted to a ternary exponential decay function: $I(t) = A + B_1e^{-t/\tau1} + B_2e^{-t/\tau2} + B_3e^{-t/\tau3}$ with the adjust R square values ($\chi^2$); $I(t)$ is the normalized time-dependent PL intensity; t is the responding time in unit of nanosecond; B is the normalized amplitude and $\tau$ is the fitted PL decay constant. The component weight of $\tau_1$ equals $B_1\tau_1/(B_1\tau_1+ B_2\tau_2+ B_3\tau_3)$. The calculation results are shown in Table S1. Transient photovoltage plots are shown in Fig. S22. The rises of photovoltage are fitted to a double exponential decay function: $V(t) = V_{eq} - B_1e^{-t/\tau1} - B_2e^{-t/\tau2}$ with the adjust R square values ($\chi^2$); $V(t)$ is the time dependent photovoltage; $V_{eq}$ is the photovoltage in equilibrium and t is the responding time in unit of microsecond.

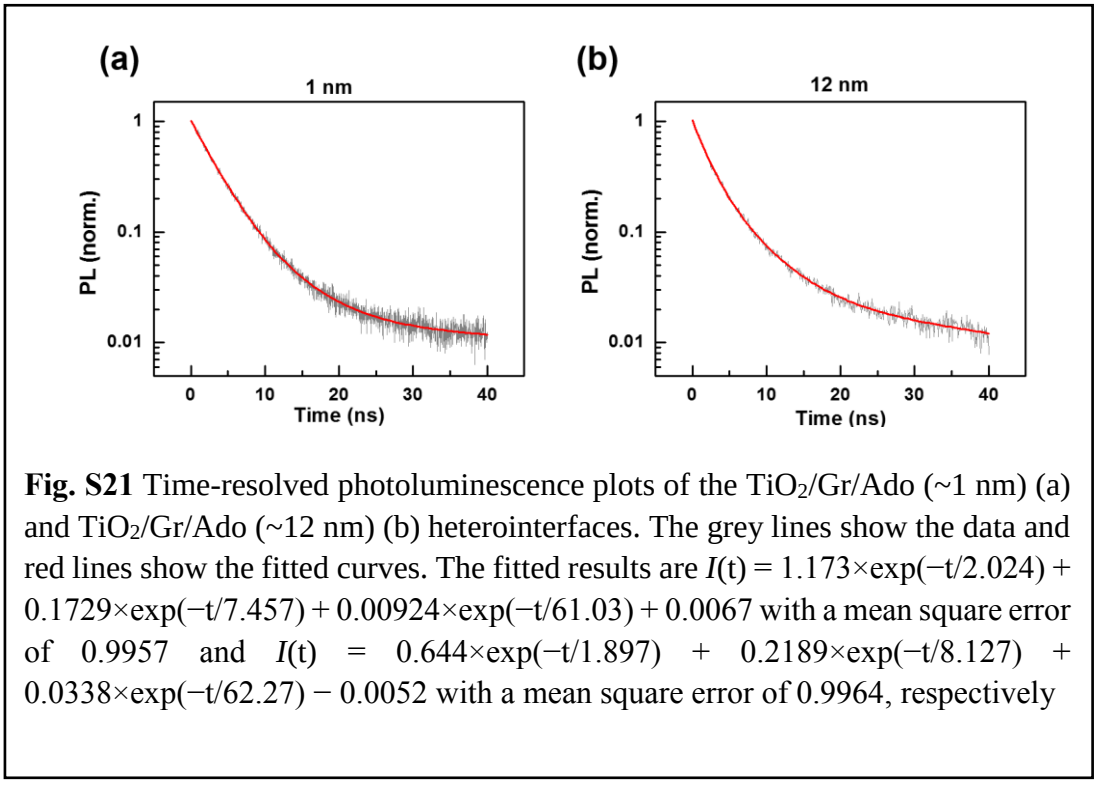


**Fig. S21** Time-resolved photoluminescence plots of the $TiO_2$/Gr/Ado (~1 nm) (a) and $TiO_2$/Gr/Ado (~12 nm) (b) heterointerfaces. The grey lines show the data and red lines show the fitted curves. The fitted results are $I(t) = 1.173\times\exp(-t/2.024) + 0.1729\times\exp(-t/7.457) + 0.00924\times\exp(-t/61.03) + 0.0067$ with a mean square error of 0.9957 and $I(t) = 0.644\times\exp(-t/1.897) + 0.2189\times\exp(-t/8.127) + 0.0338\times\exp(-t/62.27) - 0.0052$ with a mean square error of 0.9964, respectively

**Table S1.** The PL decay constants and the corresponding component weight

| Sample | $\tau_1$ (ns) | $\tau_2$ (ns) | $\tau_3$ (ns) | $\chi^2$ |
|---|---|---|---|---|
| **~1 nm Ado** | 2.024 (55.2%) | 7.457 (30.5%) | 61.03 (13.3%) | 0.9957 |
| **~12 nm Ado** | 1.897 (23.8%) | 8.127 (34.9%) | 62.27 (41.3%) | 0.9964 |

From the experimental and fitting results, it can be observed that, for the devices with ~1 nm and ~12 nm Ado, they both obey a three-exponential decay with similar $\tau$ values (See Fig. S21 and Table S1). For assigning the decay times to the different processes, we have done systematic control experiments in our previous work (Jia, C. et al. *Nano Lett.* **2016,** *16*, 3600). Time resolved PL of pure Ado shows a single exponential decay with $\tau_1 \approx 60$ ns, corresponding to the intrinsic interband recombination of Ado excitons. Time resolved PL of Ado/Graphene shows a double exponential decay, with an additional decay time $\tau_2 \approx 9$ ns, corresponding to the photo-induced electrons transfer from dye to graphene. Time resolved PL of Ado/Graphene/$TiO_2$ shows a three-exponential decay, with an additional decay time $\tau_3 \approx 2$ ns, corresponding to the charge transfer from dye to $TiO_2$. These decay times are consistent with the $\tau$ values obtained from the three-exponential fitting of ~1 nm/~12 nm $TiO_2$/Gr/Ado ternary interfaces. Thus, we can assign $\tau_1$ = ~2 ns, $\tau_2$ = ~8 ns and $\tau_3$ = ~62 ns to the mean times of photoinduced electron injection into $TiO_2$ ($\tau_1$), graphene ($\tau_2$) and the intrinsic interband recombination of Ado excitons ($\tau_3$), respectively. In addition, the photocurrent of ~1 nm/~12 nm Ado device (Fig. 3b) are 8.28/12.77 $\mu A \cdot cm^{-2}$, and for the devices with Ado thicker than 3 nm the photocurrent increases little with increasing Ado thickness. This means that the nearest 1 nm Ado dye contributes more than 60 % effective exciton. In another word, Ado dyes away from $TiO_2$/Gr/Ado ternary interface contributes little effective exciton due to the recombination processes in the Ado layer. Therefore, as in both devices Ado dye near to $TiO_2$/Gr/Ado ternary interface contribute most effective exciton for photovoltaic processes, their electron injection times are similar to each other.

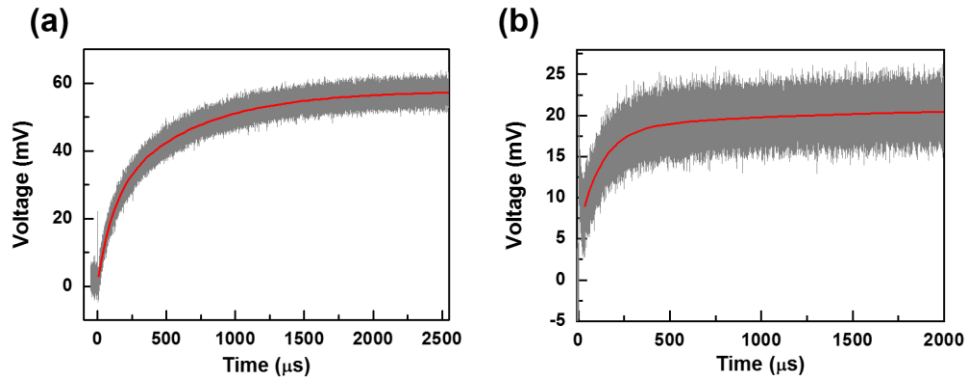


**Fig. S22** Transient photovoltage plots of the $TiO_2$/Gr/Ado (~1 nm) (a) and $TiO_2$/Gr/Ado (~12 nm) (b) heterointerfaces. The grey lines show the data and red lines show the fitted curves. The fitted results are $V = 57.80 - 33.81\times\exp(-t/602.2) - 22.85\times\exp(-t/111.7)$ with a mean square error of 0.9764 and $V = 21.08 - 2.75\times\exp(-t/1346.9) - 12.55\times\exp(-t/121.4)$ with a mean square error of 0.9607, respectively.

For the transient voltage processes in the $TiO_2$/Gr/Ado device, considering the charging processes in the In-Ag/$TiO_2$/Gr capacitor, the photovoltage generation in the $TiO_2$/Gr/Ado device contains two processes as follows. One process is photogenerated electron injection and transport on the conduction band of the $TiO_2$ layer to the In/Ag back metal electrode. As the photogenerated electron injection is very fast, this process is determined by electron transport on the conduction band of the $TiO_2$ layer to the In/Ag back metal electrode, which is independent on the thickness of the Ado dye layer and has a constant for the devices with the same $TiO_2$ layer. The other process is hole injection into the hole-collecting graphene layer, which is determined by hole transport in the Ado dye layer. This is a thickness-dependent process. The larger thickness will need the longer transport time. Through studying the control $TiO_2$/Gr/Ado devices with ~1.0 nm and ~12 nm Ado (Fig. S22), the fitted faster/slower rise times were 111.7 μs/602.2 μs for the device with ~1 nm Ado and 121.4 μs/1340.9 μs for the device with ~12 nm Ado, respectively. Therefore, it is reasonable that the faster rise time constant of ~120 μs is attributed to the thickness-independent processes of photogenerated electron injection and transport on the conduction band of the $TiO_2$ layer to the In/Ag

back metal electrode, and the slower rise time constants of ~602.2 μs/1340.9 μs for ~1.0 nm/~12 nm Ado devices correspond to the thickness-dependent process of hole injection into the hole-collecting graphene layer. In addition, from a previous work (*Nat. Mater.* **2003,** *2*, 402), Wang *et al.* have measured that the hole injection rate from single-layer Z907 dye to surrounding iodide is 30~180 μs in Z907 dye based dye-sensitized solar cells (DSSC), which indicates that hole injection has a very slow rate in a DSSC system. Considering the bad conductance and large thickness of Ado dyes, hole injection from Ado dyes to graphene with a rate of a few hundred μs is understandable.